Journal of Alloys and Compounds 909 (2022) 164679

Contents lists available at ScienceDirect

Journal of Alloys and Compounds

journal homepage: www.elsevier.com/locate/jalcom

Improving the glass forming ability and plasticity of ZrCuNiAlTi metallic glass by substituting Zr with Sc

Jiahua Zhu[a,b], Wenjin Gao[c], Sirui Cheng[a], Xiaodi Liu[a], Xiaofeng Yang[d], Jinsen Tian[a], Jiang Ma[a,e,*], Jun Shen[a,e,*]

[a] Shenzhen Key Laboratory of High Performance Nontraditional Manufacturing, College of Mechatronics and Control Engineering, Shenzhen University, Shenzhen, 518060, China
[b] Key Laboratory of Optoelectronic Devices and Systems, College of Physics and Optoelectronic Engineering, Shenzhen University, Shenzhen 518060, China
[c] Weihai Power Co., Ltd, Weifang 261061, China
[d] Science and Technology on Reliability Physics and Application of Electronic Component Laboratory, The 5th Electronics Research Institute of the Ministry of Industry and Information Technology, Guangzhou, 510610, China
[e] Guangdong Key Laboratory of Electromagnetic Control and Intelligent Robots, Shenzhen University, Shenzhen 518060, China

ARTICLE INFO

Article history:
Received 16 January 2022
Received in revised form 8 March 2022
Accepted 21 March 2022
Available online 24 March 2022

Keywords:
Bulk metallic glass
Glass forming ability
Mechanical properties
Plasticity
Free volume

ABSTRACT

The present study reports the effect of substituting Zr with Sc on the glass forming ability (GFA) and mechanical properties of ZrCuNiAlTi bulk metallic glass (BMG). Results showed that $Zr_{57-x}Cu_{20}Ni_8Al_{10}Ti_5Sc_x$ (x = 0, 1, 2, 3, 4 at%) BMGs had the best GFA at x = 2, and the critical size was 10 mm, which correlated well with the GFA indicator (T_{rg} and γ). The large atomic radius of Sc and small Gibbs free energy difference between the supercooled liquid and crystalline solid (ΔG_{l-c}) caused significant atomic size mismatch and inhibited crystallization during cooling, ultimately improving GFA. Compression test results indicated that the plasticity of the $Zr_{55}Cu_{20}Ni_8Al_{10}Ti_5Sc_2$ BMG increased fivefold (9.1%) relative to that of the Sc-free case, whereas fracture stress was successfully retained at a value of 1815 MPa. The high plastic strain of $Zr_{55}Cu_{20}Ni_8Al_{10}Ti_5Sc_2$ BMG can be attributed to the localized nanocrystallization phenomenon under uniaxial compression and to the high relaxed excess free volume (REFV) in ZrCuNiAlTiSc BMGs. The high REFV prevented the expansion of shear bands, generated secondary shear bands, and finally increased plasticity.

1. Introduction

Bulk metallic glasses (BMGs) have attracted scientific and technological interest due to their unique properties attributed to their ultrahigh strength, high hardness, good corrosion resistance, and wear resistance [1–3]. However, the two major drawbacks of BMGs are their limited glass forming ability (GFA) and poor plasticity under compressive and tensile stress at room temperature [4–7]. In contrast to dislocation multiplication in conventional alloys, localized shear bands (SBs) tend to form in BMGs due to the long-range-order disordering structures of BMGs and become the main deformation carriers during loading. Localized deformation can lead to strain softening and catastrophic failure [8–10], which limits the practical application of BMGs as structural materials. Nevertheless, extensive studies suggested that high overall plastic deformation can be achieved by increasing the number of intersecting SBs with small shear offsets. As such, effective strategies for enhancing the number of SB systems have been proposed, such as (i) in situ or ex situ formation of BMG composites in which second crystalline phases are embedded in BMG matrices [11–16]; (ii) design of BMGs with high Poisson's ratio [4, 17–19]; and (iii) introduction of free volume through deformation, fast cooling, or microalloying [20–25]. Microalloying or minor addition is a simple and effective way to enhance the GFA and plasticity of BMGs. Elements that have large negative heat of mixing and common base elements improve the GFA or plasticity of BMGs [23, 26–32]. For instance, the substitution of Zr with Al can stabilize the short-range order structure and improve the GFA, crystallization activation energy, and mechanical properties of Zr-based BMGs [23]. Jiang et al. [26] fabricated a CuZr-based BMG with high strength and excellent compressive plastic strain of up to 32.5% through 2 at% Ti alloying. Their results indicated that the origin of high plasticity is the increase in free volume after Ti addition [26]. Similar results can be observed in other BMGs [21,27]. Furthermore, microalloying leads to changes in atomic or

* Corresponding authors at: College of Mechatronics and Control Engineering, Shenzhen University, Shenzhen, Guangdong 518060, China.
E-mail addresses: majiang@szu.edu.cn (J. Ma), junshen@szu.edu.cn (J. Shen).

https://doi.org/10.1016/j.jallcom.2022.164679
0925-8388/

electronic structures and induces the simultaneous formation of different kinds of atomic bonds, which in turn promote the plasticity of BMGs [28].

In the past decades, the effects of rear-earth (RE) element addition on the glass forming ability and plasticity of different BMG systems have been extensively studied [29–33]. The RE elements Sc exhibits a great potential as an enhancer of the GFA and plasticity of BMGs. Zhang et al. [32] reported that a fourfold enhancement in ductility (1.5–5.9%) can be achieved in Ti-Cu-Zr-Fe-Sn-Si BMGs through 2 at% Sc addition. With regard to Zr-based BMGs, most studies mainly focused on the effect of Sc addition on GFA, whereas the impact of the process on plasticity behavior is rarely reported [29, 34–36]. In this study, a ZrCuNiAlTi BMG-forming alloy was used as a base alloy [37], and the roles of Sc addition in the GFA and mechanical properties of $Zr_{57-x}Cu_{20}Ni_8Al_{10}Ti_5Sc_x$ (x = 0, 1, 2, 3, 4 at%) alloys were systematically investigated.

2. Materials and methods

$Zr_{57-x}Cu_{20}Ni_8Al_{10}Ti_5Sc_x$ (x = 0, 1, 2, 3, 4 at%) alloy ingots, labeled as Sc0, Sc1, Sc2, Sc3, and Sc4, were prepared by arc-melting high-purity Zr (97.5 wt%), Cu (99.9 wt%), Ni (99.9 wt%), Al (99.9 wt%), Ti (99.9 wt %), and Sc (99.9 wt%) in a water-cooled copper hearth in a Ti-gettered high-purity argon atmosphere. Chemical homogeneity was ensured by re-melting the ingots at least five times. Rod samples that were 2 mm in diameter and 80 mm in length were fabricated through copper mold casting.

Phase identification of the as-prepared alloys was analyzed on the X-ray diffraction (XRD, Rigaku MiniFlex 600) with Cu-K_α radiation at a voltage of 40 kV. The glassy phase was examined through high-resolution transmission election microscopy (HRTEM, JEOL F200) at an acceleration voltage of 200 kV. Samples for transmission electron microscopy (TEM) analysis were prepared using Precision Ion Polishing System (GATAN PIPS II 695) with 3.0 keV Ar^+ ions in a liquid nitrogen environment. Thermal properties associated with glass transition (T_g), crystallization (T_x), melting (T_m), and liquid temperature (T_l) were measured through differential scanning calorimetry (DSC, Netzsch STA 404F3) at a heating rate of 20 K/min. The specific heat capacity (C_p) of the amorphous phase was measured using DSC-404F3, and the measurement was based on the comparison with the specific heat capacity of a sapphire standard sample. All measurements were performed using argon gas at a heating rate of 20 K/min in PtRh pans on C_p measurement mode. The cylinder samples (2 mm in diameter and 6 mm in height) were used for the viscosity and linear thermal expansion measurements, which were performed with a thermal mechanical analyzer (TMA, Netzsch TMA 402) at a heating rate of 5 K/min under a compressive load of 3 N. Cylindrical rods (2 mm in diameter and 4 mm in height) were used to measure room-temperature compressive mechanical properties with an Instron testing machine at a strain rate of ~5×10^{-4}/s. The fracture surfaces of the deformed samples were observed with scanning electron microscopy (SEM, FEI Quanta 450FEG).

3. Results

Fig. 1a shows the XRD patterns of the as-cast Sc0-Sc4 rods with diameters of 2 mm. The diffraction patterns of the prepared samples exhibit only a distinct diffraction halo at 2θ of 38° and have no detectable Bragg peaks corresponding to the crystalline phase, indicating their glassy structures. The HRTEM image and corresponding selected area diffraction pattern (SADP) of Sc0, Sc2, and Sc4 rods are shown in Fig. 1b, Fig. 1c, and Fig. 1d, respectively. The HRTEM images of all samples show typical amorphous structures with isotropic maze patterns and show no crystalline phases. Furthermore, the SADP in the inset of Fig. 1b–d displays a typical

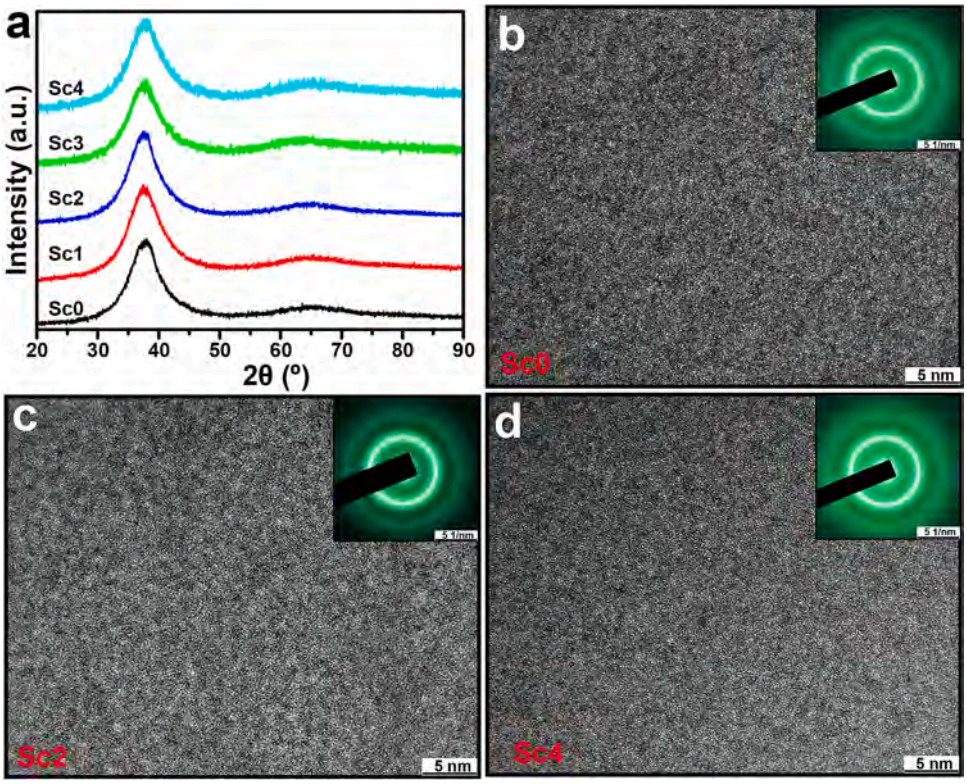

Fig. 1. (a) XRD patterns of the as cast Sc0-Sc4 samples with a diameter of 2 mm. (b-d) HRTEM and the corresponding SADP (in the inset) images of the prepared Sc0, Sc2 and Sc4 rods.

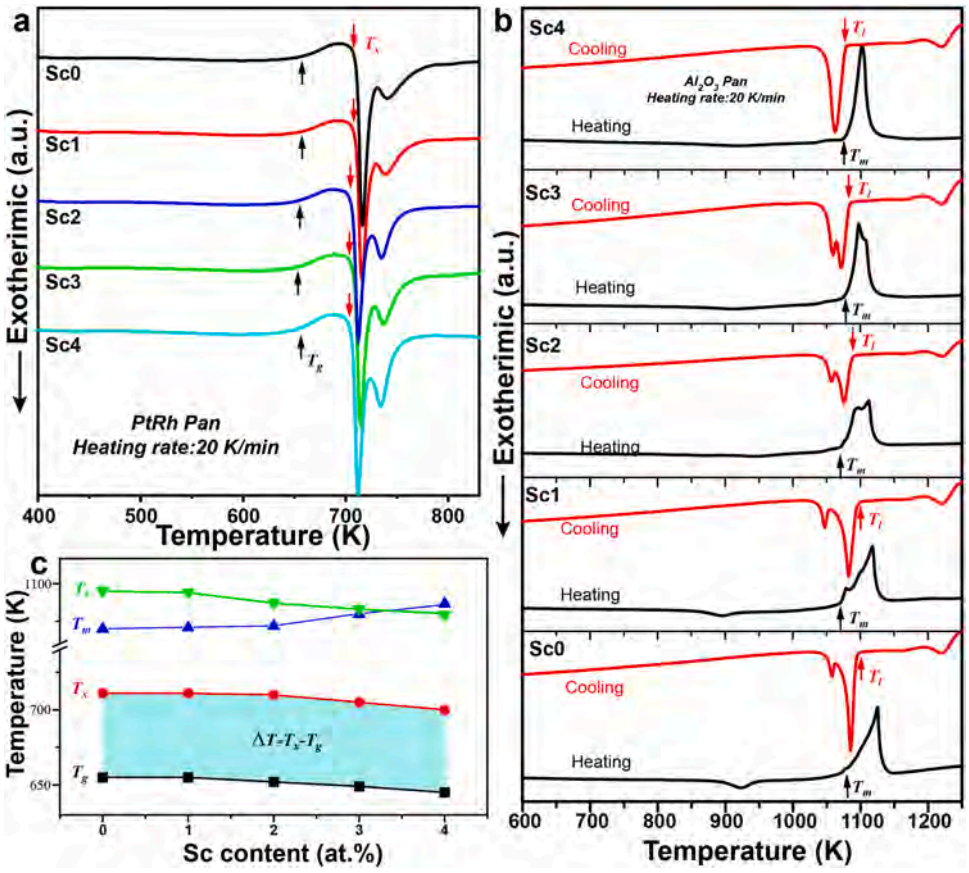

Fig. 2. DSC curves of as cast Sc0-Sc4 rods at a heating rate of 20 K/min. (a) 400–830 K by using PtRh pan, (b) 600–1250 K by using Al_2O_3 pan. (c) T_g, T_x, T_m, T_g and ΔT (blue area) as a function of Sc content for the ZrCuNiTiAlSc alloys.

amorphous halo ring and has no diffraction spots, indicating the glassy nature of the Sc0, Sc2, and Sc4 rods.

Fig. 2a presents the DSC curves obtained from as-cast samples with diameters of 2 mm (Sc0–Sc4) from 400 K to 830 K at a constant heating rate of 20 K/min. All DSC curves exhibit a distinct endothermic event corresponding to glass transition (T_g) and followed by a supercooled liquid region ($\Delta T = T_x$-T_g) before crystallization (T_x). The characteristic temperatures (T_g and T_x) were marked by arrows. The melting transformation of the BMGs (Sc0–Sc4) was measured using DSC, and the curves are shown in Fig. 2b. The onset melting temperature (T_m) and liquidus temperature (T_l) were determined from the heating and cooling curves, respectively. The sample subjected to the low temperature test (400–830 K) was used in determining T_m and T_l. As shown in Fig. 2b, in contrast to the two melting stages of Sc0, Sc1, Sc2, and Sc3 alloys, the melting stage of Sc4 has only one melting peak, which indicates that Sc4 is close to the eutectic point. The T_g, T_x, ΔT, T_m and T_l of the BMG alloys are plotted in Fig. 2c and summarized in Table 1. The T_g, T_x, and T_m values gradually decrease with increasing Sc content, T_l increases slightly, and ΔT hardly changes. In general, ΔT is positively correlated with GFA. However, in the ZrCuNiTiAlSc system, ΔT is hardly affected by Sc content. The relationship between ΔT and GFA will be discussed in detail in subsequent sections. The XRD, TEM, and DSC results show that all the alloys are in a fully amorphous state.

Fig. 3 shows the typical room temperature compressive stress–-strain curves of the Sc0, Sc1, Sc2, Sc3, and Sc4 alloy rods at a strain rate of 5×10^{-4}/s. The yield stress (σ_y) and plastic strain (ε_p) are summarized in Table 2. The addition of Sc has an obvious effect on σ_y

Table 1
Characteristic temperatures T_g, T_x, T_m, and T_l, the parameters $\Delta T_x = T_x$-T_g, $T_{rg} = T_g/T_l$, $\gamma = T_x/(T_g + T_l)$, $\gamma_m = (2T_x$-$T_g)/T_l$, $\delta = T_x/(T_l$-$T_g)$, $K_{gl} = (T_x$-$T_g)/(T_m$-$T_x)$ and $\omega = T_g/T_x$-$2T_g/(T_g$-$T_l)$ for all $Z_{57\text{-}x}Cu_{20}Ni_8Al_{10}Ti_5Sc_x$ (x = 0, 1, 2, 3 and 4 at%) alloys.

Alloys	T_g (K)	T_x (K)	T_m (K)	T_l (K)	ΔT_x (K)	T_{rg}	γ	γ_m	δ	K_{gl}	ω
Sc0	655	711	1070	1095	56	0.5982	0.4063	0.7005	1.6159	0.1560	0.1727
Sc1	655	711	1071	1094	56	0.5987	0.4065	0.7011	1.6196	0.1556	0.1722
Sc2	652	710	1072	1087	58	0.5998	0.4083	0.7065	1.6322	0.1602	0.1685
Sc3	649	705	1088	1083	56	0.5993	0.4070	0.7027	1.6244	0.1493	0.1711
Sc4	645	700	1086	1080	55	0.5972	0.4058	0.6991	1.6092	0.1425	0.1736

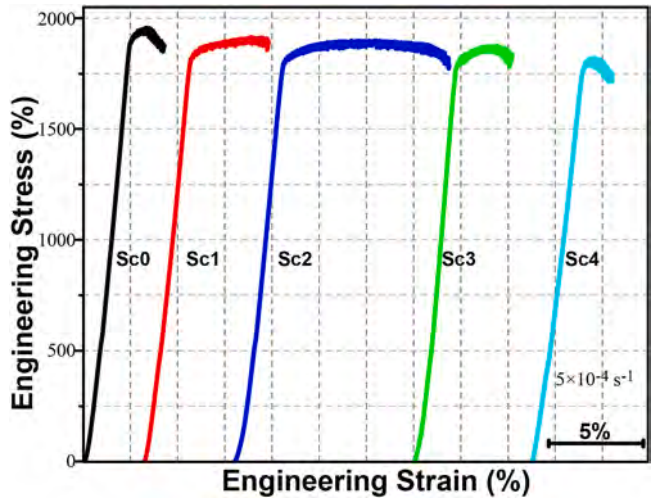

Fig. 3. Compressive strain–stress curves of the cast Sc0-Sc4 BMG rods (2 mm in diameter and 4 mm in length) at a stain rate of 5×10^{-4} s^{-1} at room temperature.

and ε_p. The plasticity of the Sc1 and Sc2 BMGs significantly improves. Specifically, compared with the ductility of the Sc-free sample, the ductility of the Sc2 alloy increases of about 9.1% while a strength of 1815 MPa is maintained. However, as Sc content continuously increases (> 2 at%), the plasticity of present BMGs gradually decreases. The plasticity sequence is Sc2 > Sc1 > Sc3 > Sc0 > Sc4. In addition, Sc-based BMGs have lower fracture strength than other BMG-forming systems [30]. Hence, σ_y decreases with increasing Sc content in the ZrCuNiTiAlSc BMGs.

Fig. 4 shows the SEM images of Sc0, Sc2, and Sc4 BMG rods after fracture in compression test. Apparently, the number of SBs in the prepared BMGs varies in the enlarged view of the fracture lateral surface. In the Sc0 alloy, straight SBs can be observed on the surface (Fig. 4a). A high density of multiple SBs marked by red and yellow arrows appears on the surface of the Sc2 rod (Fig. 4c). These SBs branch and interact with one another (marked by red circles in Fig. 4c), and the interactions prevent the rapid expansion of the main SBs along a single direction. When the Sc content was increased to 4 at%, as shown in Fig. 4e, the characteristics of the SBs are similar to those of the Sc0 alloy. The plastic is accommodated through the generation of multiple SBs [38]. The above results indicate that the Sc2 alloy has the largest number of nucleation sites of SBs among the ZrCuNiTiAlSc BMGs, consistent with the large plastic deformation. Fig. 4b and Fig. 4f show the fracture surfaces of Sc0 and Sc4 BMGs, respectively. The alloys exhibit vein-like patterns and many smooth regions, which is a typical fracture of BMG. In sharp contrast, the fracture surfaces of Sc2 (Fig. 4d) BMG display a vein-like patterns without smooth regions because the SBs proliferate and change during SB propagation. Similar results were observed in other BMGs with good compression plasticity [39,40].

4. Discussion

4.1. Effect of substitute Zr with Sc on GFA

From the experimental data (Fig. 2a-b), the empirical parameters of GFA, i.e., ΔT, T_{rg}, γ, γ_m, δ, K_{gl} and ω, are derived and listed in Table 1. Although the ΔT does not change significantly in all the alloys, the T_{rg}, γ, γ_m, δ, K_{gl} and ω parameters are markedly different. Among all BMGs, Sc2 BMG has the largest T_{rg}, γ, γ_m, δ, K_{gl} values and minimum ω value, and thus exhibits excellent GFA. In a multicomponent system, atomic size mismatch of > 12% and elements with negative heat of mixing are the two main factors affecting GFA [2]. In the ZrCuNiAlTiSc system, although the enthalpy of mixing Sc and Zr is positive (Fig. 5a), atomic size mismatch can be significantly increased when the large atoms of Sc (0.162 nm) replaces Zr given that Sc can prevent the long-range diffusion of constituent atoms and enhance GFA. In addition, the heat of formation of scandium oxide (1909.85 kJ/mol) [41] is much higher than that of ZrO (1102.3 kJ/mol) [42]. Hence, Sc can easily react with oxygen in liquid state and produce Sc_2O_3, which can absorb oxygen from alloy melts, purify alloy melts, reduce heterogeneous nucleation, and consequently improve GFA. Furthermore, it is well known that many of the BMG compositions with the best GFA are not eutectic point compositions, but the composition that slightly deviate from the eutectic point [43]. Similarly, in the melting process of ZrCuNiAlTi system (see in Fig. 2. b and Fig. 2. c), it can be seen that the composition of Sc4 alloy is closer to the eutectic point than that of Sc2 alloy, which further indicates that the GFA of the Sc2 alloy is higher than that of Sc4. In addition, Hu et al. [44] reveal that microalloying to glass forming alloys can induce strong chemical frustration other than topological frustration, which is crucial to promote the GFA. This is another important reason for the high GFA of Sc2 BMG.

For the analysis of the effect of Sc addition on the GFA of ZrCuNiAlTi BMGs, difference in Gibbs free energy between the supercooled liquid and crystalline solids (ΔG_{l-c}) were calculated using the following expression [45]:

$$\Delta G_{l-c} = \frac{\Delta H_m (T_m - T)}{T_m} - \frac{\gamma \Delta H_m}{T_m}\left[\left(T_m - T\right) - T\ln\left(\frac{T_m}{T}\right)\right]$$

where ΔH_m is the heat of fusion and T_m and γ are the melting temperature and proportionality coefficient, respectively. In the metallic glass forming liquids, the γ value is generally 0.8 [45]. Fig. 5c shows the calculated ΔG_{l-c} as a function of temperature normalized to the melting temperature of the BMGs. The ΔG_{l-c} of the Sc2 BMG is the smallest under any given undercooling condition, implying that the Sc2 BMG forming melt can stabilize the liquid state during cooling, inhibit crystallization, and finally achieves a high GFA.

The results discussed from the characteristic parameters (ΔT, T_{rg}, γ, γ_m, δ, K_{gl} and ω) and ΔG_{l-c} were verified. Accordingly, Sc2 and Sc0 alloys with different sizes were prepared, and their structures were determined. The results are shown in Fig. 6. The XRD patterns of Sc0

Table 2
Summary of the exothermic peak area (ΔH_{fv}) before T_g, relaxed excess free volume (REFV) and mechanical properties of the $Zr_{57-x}Cu_{20}Ni_8Al_{10}Ti_5Sc_x$ (x = 0, 1, 2, 3 and 4 at%) BMGs.

Alloys	ΔH_{fv} (J/g)	ΔH_m (J/g)	REFV (%)	σ_f (MPa)	ε_p (%)
Sc0	-4.12	104.4	0.19	1907 ± 25	1.8 ± 0.3
Sc1	-5.61	116.7	0.33	1857 ± 20	5.4 ± 0.4
Sc2	-6.35	125.8	0.39	1815 ± 30	9.1 ± 0.6
Sc3	-4.63	129.4	0.24	1770 ± 25	3.0 ± 0.3
Sc4	-3.94	138.2	0.21	1750 ± 30	1.9 ± 0.2

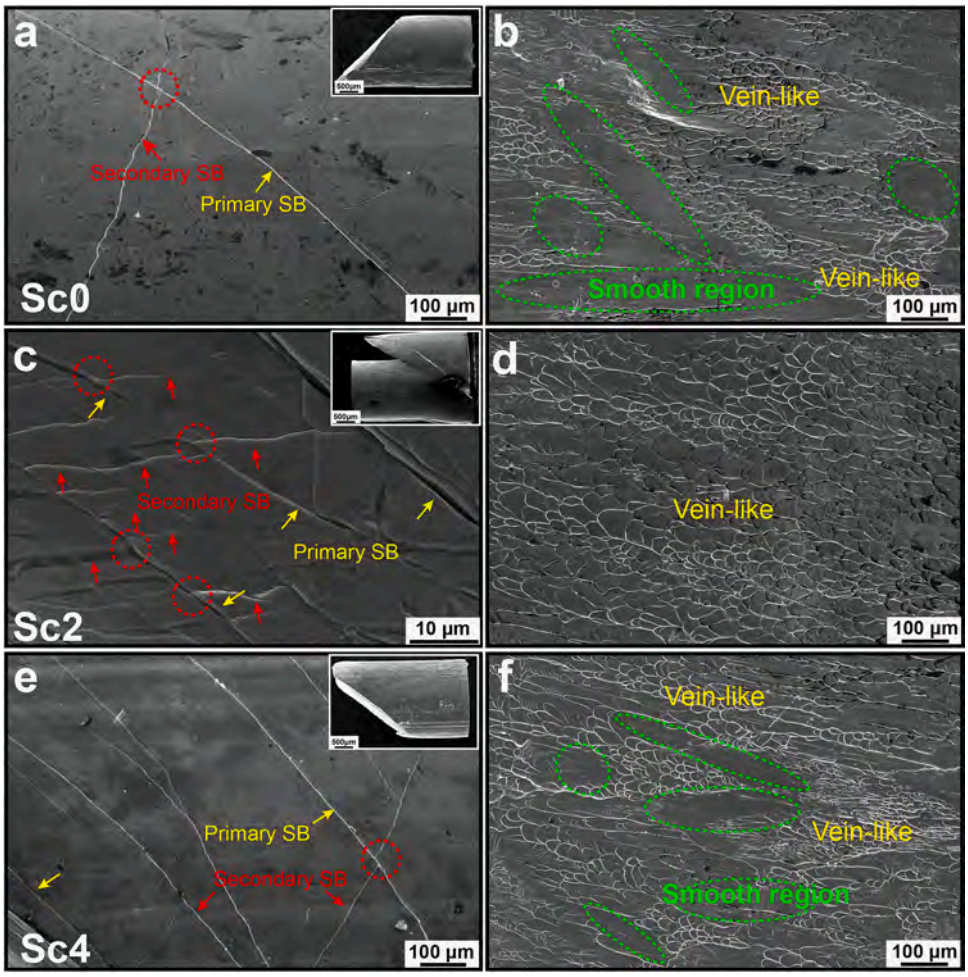

Fig. 4. SEM images of the fracture surfaces for the cast ZrCuNiTiAlSc BMG rods in compressive deformation mode: (a-b) Sc0; (c-d) Sc2 and (e-f) Sc4.

(3 mm) and Sc2 (10 mm) BMGs consist of only a broad halo without discernible crystalline peaks. This result further confirms that the substitution of Zr with Sc can greatly improve the GFA of ZrCuNiAlTi BMGs. Herein, the critical diameter of Sc0 BMG is 3 mm possibly because of the low purity of Zr.

4.2. Origin of the effect of substitution Zr with Sc on plasticity

Lewandowski et al. [17] reported that the plasticity of BMG correlates with its Poisson's ratio ν or a ratio of shear modulus G to bulk modulus B (G/B). The larger the ν (> 0.31–0.32) is, the more ductile the BMGs have. In the present work, owing to the small critical diameters of the prepared BMGs, obtaining accurate modulus data with experimental methods is difficult. Herein, the moduli of ZrCuNiTiAlSc BMGs were calculated by using an empirical formula [46,47].

$$M^{-1} = \sum f_i M_i^{-1}$$

where M_i and f_i are the elastic constant and the atomic percentage of the consistent element, i, respectively. The elastic constant data of the base elements for ZrCuNiAlTiSc BMGs at room temperature are obtained from Ref [4]. After the B and G of ZrCuNiAlTiSc BMGs are calculated, ν can be derived from $\nu = \frac{1}{2}(3B - 2G)/(3B + G)$. As shown in Fig. 7, the calculated Poisson's ratio (ν) of each ZrCuNiAlTiSc BMG decreases with increasing Sc content because of the relatively low ν value of Sc element. Thus, Poisson's ratio is not the main reason for the improved plasticity after the minor addition of Sc to the BMGs.

For the analysis of the origin of the high plasticity of the Sc2 alloy, the microstructure after the compression of the typical alloys was systematically studied. Fig. 8 shows the HRTEM image and SADP (the inset) of the fractured Sc0, Sc2, and Sc4 alloy rods in the SB regions that formed near the compressive fracture surface (Figs. 4a, 4c and 4e). In the Sc0 and Sc4 alloys (Figs. 8a and 8c), only a unique microstructure consisting of a 10 nm-wide SB can be clearly observed, and no nanocrystalline phase were detected in and out of the SB, indicating that the Sc0 and Sc4 BMGs after compression deformation retain fully homogeneous glassy structures. However, in Sc2, a small number of nanocrystallites are distributed near the shear bands with different sizes, as shown in Fig. 8b. The SADPs corresponding to the

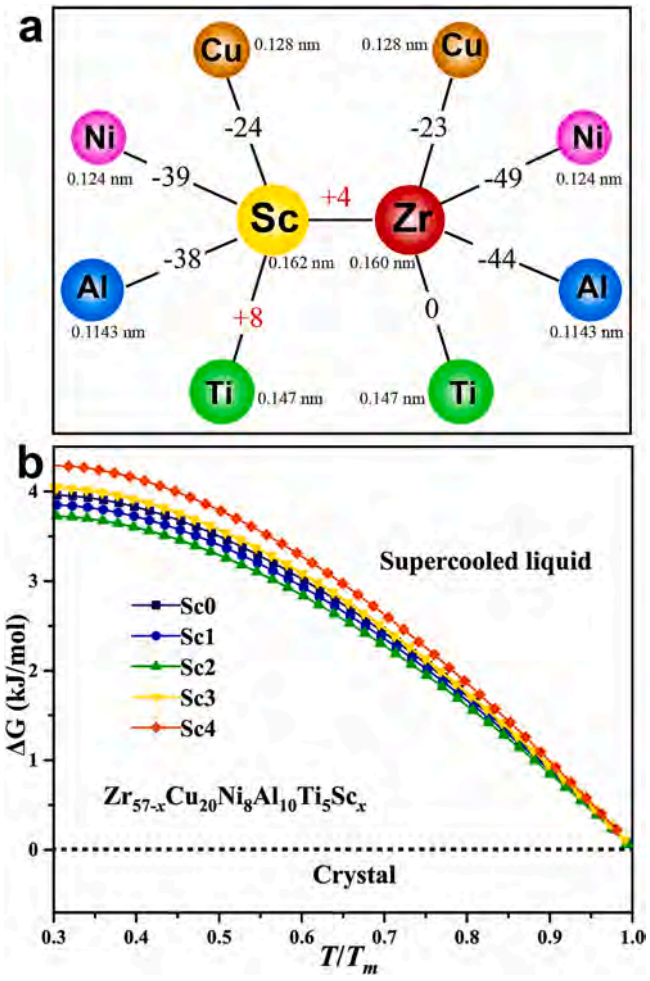

Fig. 5. (a) Atomic radius and the heats of mixing between two elements in ZrCuNiTiAlSc system. (b) Gibbs free energy difference between supercooled liquid state and crystal state as a function of temperature for the ZrCuNiTiAlSc BMGs.

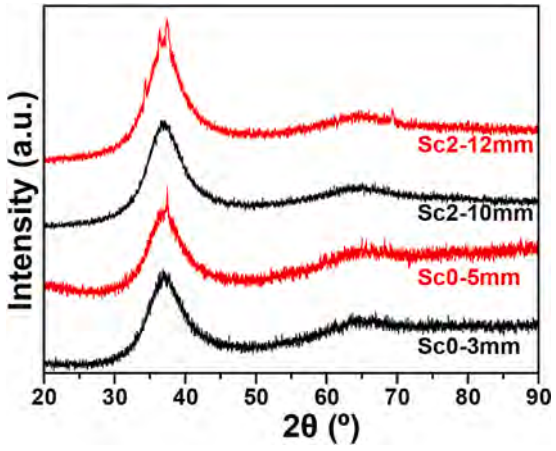

Fig. 6. XRD patterns of the Sc0 and Sc2 alloys with different diameters.

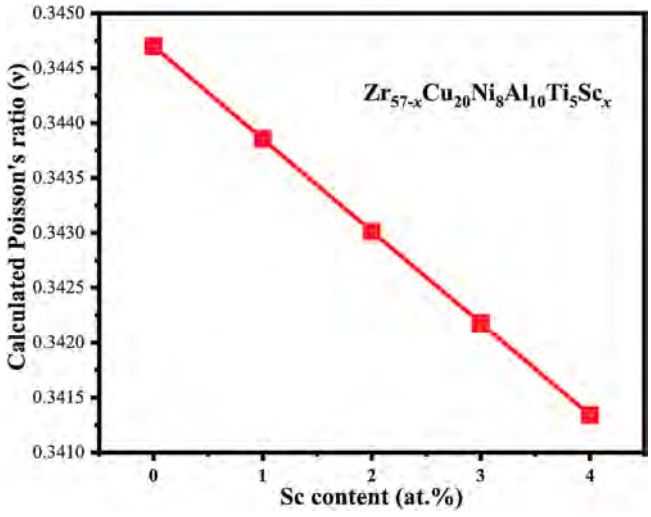

Fig. 7. Poisson's ratio (ν) of Sc0-Sc4 BMGs calculated using the empirical formula.

regions "A" and "B" (in the inset of Fig. 8b) further confirm the presence of the nanocrystallites and indicates that deformation indeed facilitates nanocrystallization. In the Cu–Zr containing BMGs, compressive loading can facilitate nanocrystallization and result in plasticity [48]. Although no obvious SB branching occurs in the Sc2 BMG, a curved shear band induced by nanocrystals appears. In the HRETM image in Fig. 1c, the high plasticity of the as-cast Sc2 BMG is caused by nanocrystalline phase formation in the SB during deformation. Although the Sc2 BMG shows nanocrystallization behavior after deformation, the cause of the nanocrystallization is unclear.

According to the free volume model and flow unit model, the BMGs are not in a completely densely packed state, and the distribution of defects (free volume and nano-scale liquid like flow units) in BMGs is random, and heterogeneous free volume in MGs is uniformly distribution [49]. Wang et al. [49] found that free volumes are typically not distributed homogeneously in BMGs and are mainly enriched in the areas of flow units. Gulzar et al. [50] reported that atoms in a flow unit easily move to a stable position in the form of nucleation site and then grow to form nanocrystals during crystallization. In other words, flow units where free volumes are enriched likely undergo crystallization during compression deformation, thereby changing the deformability of BMGs. In the present work, the cause of the large plastic strain of the Sc2 BMG was determined on the basis of the REFV of ZrCuNiTiAlSc BMGs. The REFV was determined using two methods. First, the broad exothermic peak before T_g is closely correlated to REFV in BMGs [20,22,26], as indicated by the equation $\Delta H_{fv} = \beta \cdot \Delta v_f$ [51,52], where β is a constant and Δv_f is the change in REFV per atomic volume. This equation indicates a positive correlation between ΔH_{fv} and REFV. The relative content of the REFV of ZrCuNiTiAl BMG under the same test conditions could be quantitatively estimated by measuring the release enthalpy below the T_g [53–55]. For the calculation of ΔH_{fv}, the specific heat capacity (C_p) of each ZrCuNiAlTiSc BMG was calculated through DSC measurement at a heating rate of 20 K/min, as shown in Figs. 9a and 9b. Compared with the Sc free alloy, the Sc1 and Sc2 alloys have negative ΔH_{fv} values of approximately − 5.61 and − 6.35 J/g, respectively. All

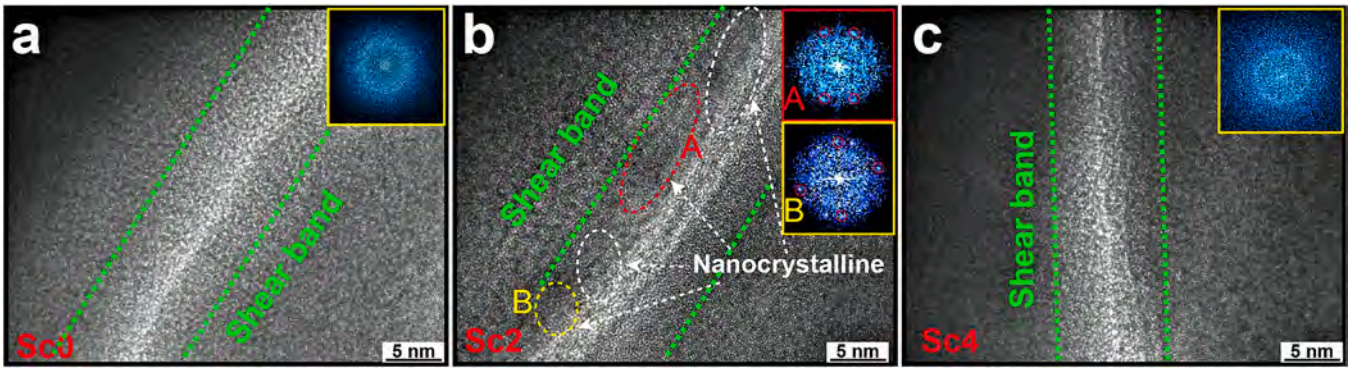

Fig. 8. (a-c) HRTEM and the corresponding SADP (in the inset) images of the Sc0, Sc2 and Sc4 rods after compressive test, respectively.

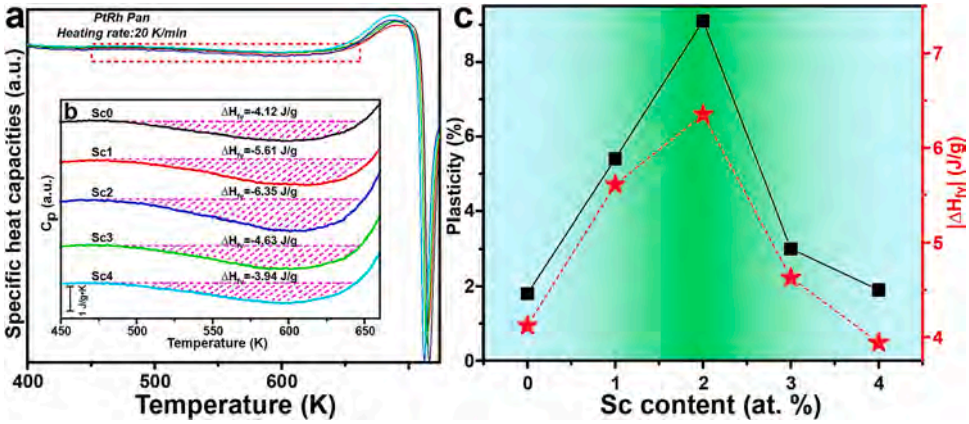

Fig. 9. (a) Specific heat capacities (C_p) of Sc0-Sc4 BMGs, and the magnified views of the thermograms indicating structural relaxation are inset (b). (c) Relationships between ΔH_{fv} and plasticity with Sc contents.

the ΔH_{fv} values and the corresponding plasticity of the BMGs are plotted in Fig. 9c. The trend of plasticity versus Sc content is consistent with the changes in REFV versus Sc content in the BMGs.Fig. 10.

Another efficient way to determine the REFV of BMGs is measuring the difference of thermal expansion before and after structural relaxation [21,56]. Fig. 10a-g show the normalized length change ($\Delta l/l_0$, the length change divided by the initial length) as a function of temperature for Sc0, Sc1, Sc2, Sc3 and Sc4 BMGs. In these curves, the whole process of determining the REFV can be divided into three parts: (1) the first heating at a rate of 5 K/min starts from room temperature to the temperature just below the T_g, and then the final temperature is held for 60 min for complete structural relaxation; (2) cooling at the same rate to room temperature; (3) confirmation of the completion of structural relaxation. The second heating at a rate of 5 K/min starts from room temperature to the temperature higher than T_x. The REFV can be expressed as volume shrinkage, which is three times the $\Delta l/l_0$, caused by the structural relaxation below T_g [21,56]. In the ZrCuNiTiAlSc system, the relationships between the REFV and plasticity with Sc content are shown in Fig. 10h. The REFV and plasticity increase first and then decrease with increasing of Sc content. This behavior is identical to the observed when the ΔH_{fv} method is used. The Sc1 and Sc2 BMGs exhibit plasticity of more than 5% when the REFV exceeds 0.3%. These results suggest that a high REFV in the Sc2 BMG enhances plasticity.

The microstructure of BMG can be considered as a composite consisting of liquid-like regions embedded in the continuous elastic backbone regions [4,5,57]. The atoms in the liquid-like zone packed more loosely and containing a high density of REFV, which was benefit for the atomic arrangement and further promoting the nucleation of SBs [58,59]. Generally, the formation, morphology and propagation of SBs plays an important role in the deformation of BMGs. For the Sc2 BMG, the high plasticity is considered to be originated from the higher REFV (Fig. 9b and Fig. 10f) and the nanocrystallization (Fig. 8b) near the SBs. Both the high REFV and nanocrystallines formation during the deformation process improve the nucleation of SBs. And during the propagation of SBs, as shown

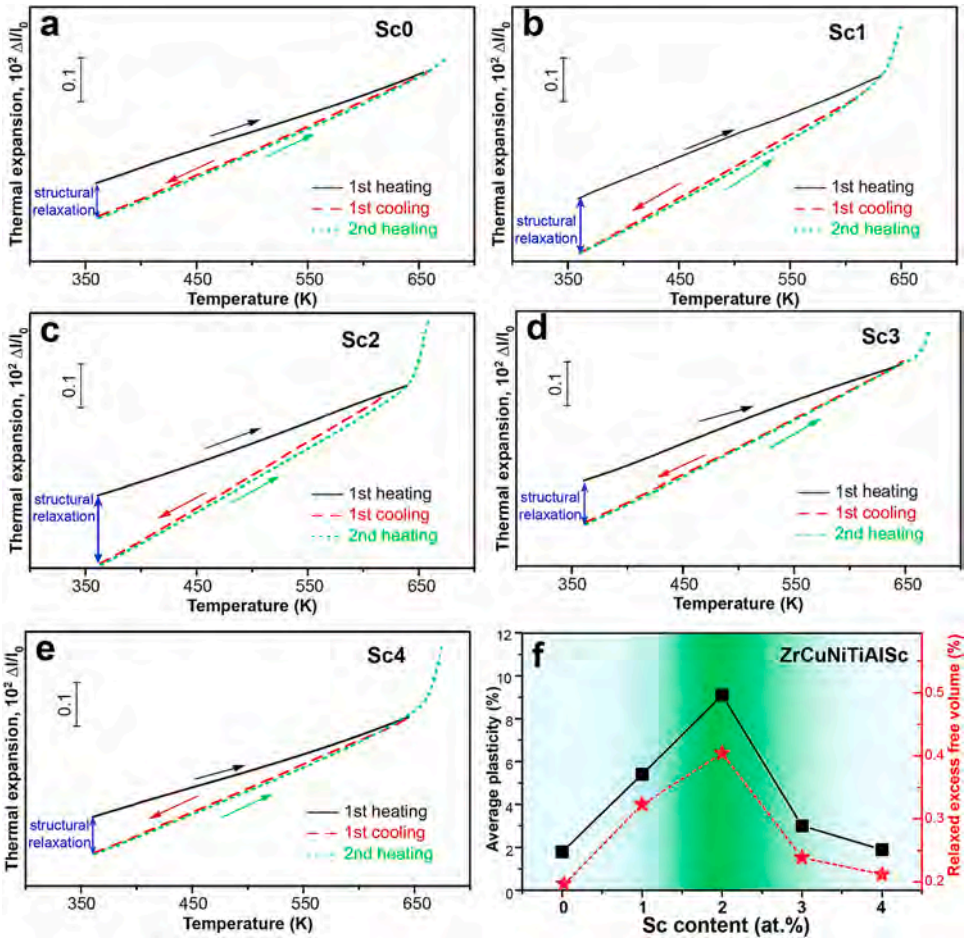

Fig. 10. (a)-(g) show the length change (Δl) normalized with the initial length ($\Delta l/l_0$), versus temperature for Sc0 to Sc4 BMGs. (h) Relationships between the REFV and plasticity with Sc content.

in Fig. 4c, the previously formed SBs of Sc2 BMG are subsequently deflected by the obstruction of the nanocrystallines, which leads to the formation of new SBs. As a result, the Sc2 BMG exhibits a large number of shear bands during deformation, which ultimately increases its plasticity.

5. Conclusions

In summary, the influences of the partial substitution of Zr with Sc on GFA and compressive mechanical properties of $Zr_{57-x}Cu_{20}Ni_8Al_{10}Ti_5Sc_x$ ($x = 0$, 1, 2, 3, 4 at%) glassy alloys were investigated. The results were summarized as follows:

(1) 2 at% Sc substitution Zr can effectively improve the GFA with critical diameter at least 10 mm. Although the addition of Sc can enhance the Trg and γ values, it has little effect on the supercooled liquid region (ΔT).
(2) The large atomic radius of Sc addition can significantly increase the atomic size mismatch and inhibit the long-range diffusion of atoms during cooling and finally retains the amorphous structure. Additionally, the ΔGl-c of the Sc2 glassy forming alloy is the smallest. This feature is another reason for the high GFA of the Sc2 BMG.
(3) The Sc2 BMG exhibits the highest plasticity of approximately 9.1%, which is five times that of Sc-free BMGs. The HRTEM results of the Sc2 BMG after compression illustrate that the high plastic strain is caused by the occurrence of nanocrystals during deformation and without phase separation phenomenon.
(4) Further analysis indicates that the high plasticity of the Sc2 alloy is due to the large number of REFVs (determined by DCS and TMA), which may serve as nucleation sites for the precipitation of nanocrystals during compression deformation. These nanocrystals promote SB interaction and the branching and formation of secondary SBs, which ultimately improve plasticity.

CRediT authorship contribution statement

Jiahua Zhu: Conceptualization, Formal testing & analysis, Methodology, Writing - Original Draft. **Wenjin Gao:** Formal testing & analysis, Writing - Original Draft. **Sirui Cheng:** Formal testing & analysis. **Xiaodi Liu:** Methodology, Writing - Review & Editing. **Xiaofeng Yang:** Investigation. **Jinsen Tian:** Data curation, Writing - Review & Editing. **Jiang Ma:** Supervision, Writing - Review & Editing. **Jun Shen:** Supervision, Writing - Review & Editing.

Declaration of Competing Interest

The authors declare that they have no known competing financial interests or personal relationships that could have appeared to influence the work reported in this paper.

Acknowledgements

This work was financial supported by the China National Natural Science Foundation of China (No. 52071217), the National Key

Research and Development Program of China (No. 2018YFA0703605), the Guangdong Key Laboratory of Electromagnetic Control and Intelligent Robots and the China Postdoctoral Science Foundation (No. 2021M700872) The authors are grateful for the technical assistance from the Instrumental Analysis Center of Shenzhen University.

References

[1] M.D. Demetriou, M.E. Launey, G. Garrett, J.P. Schramm, D.C. Hofmann, W.L. Johnson, R.O. Ritchie, A damage-tolerant glass, Nat. Mater. 10 (2011) 123–128.
[2] A. Inoue, Stabilization of metallic supercooled liquid and bulk amorphous alloys, Acta Mater. 48 (2000) 279–306.
[3] C.A. Schuh, T.C. Hufnagel, U. Ramamurty, Mechanical behavior of amorphous alloys, Acta Mater. 55 (2007) 4067–4109.
[4] W.H. Wang, The elastic properties, elastic models and elastic perspectives of metallic glasses, Prog. Mater. Sci. 57 (2012) 487–656.
[5] J.C. Qiao, Q. Wang, J.M. Pelletier, H. Kato, R. Casalini, D. Crespo, E. Pineda, Y. Yao, Y. Yang, Structural heterogeneities and mechanical behavior of amorphous alloys, Prog. Mater. Sci. 104 (2019) 250–329.
[6] Yu Chen, Chunguang Tang, Jian-Zhong Jiang, Bulk metallic glass composites containing B2 phase, Prog. Mater. Sci. 121 (2021) 100799.
[7] J. Schroers, W.L. Johnson, Ductile bulk metallic glass, Phys. Rev. Lett. 93 (25) (2004) 255506.
[8] A.L. Greer, J.J. Lewandowski, Temperature rise at shear bands in metallic glasses, Nat. Mater. 5 (1) (2005) 15–18.
[9] D. Rodney, C. Schuh, Distribution of thermally activated plastic events in a flowing glass, Phys. Rev. Lett. 102 (23) (2009) 235503.
[10] S. Pauly, S. Gorantla, G. Wang, U. Kühn, J. Eckert, Transformation-mediated ductility in CuZr-based bulk metallic glasses, Nat. Mater. 9 (6) (2010) 473.
[11] D.C. Hofmann, Shape memory bulk metallic glass composites, Science 329 (5997) (2010) 1294–1295.
[12] Y. Wu, Y. Xiao, G. Chen, C.T. Liu, Z. Lu, Bulk metallic glass composites with transformation-mediated work-hardening and ductility, Adv. Mater. 22 (25) (2010) 2770.
[13] J. Qiao, H. Jia, P.K. Liaw, Metallic glass matrix composites, Mater. Sci. Eng. R Rep. 100 (2016) 1–69.
[14] W. Song, Y. Wu, H. Wang, X. Liu, H. Chen, Z. Guo, Z. Lu, Microstructural control via copious nucleation manipulated by in situ formed nucleants: large-sized and ductile metallic glass composites, Adv. Mater. 28 (37) (2016) 8156.
[15] R. Wei, L.B. Chen, H.P. Li, F.S. Li, Compression-compression fatigue behavior of CuZr-based bulk metallic glass composite containing B2 phase, Intermetallics 85 (2017).
[16] T. Li, Y. Liao, S. Song, Y. Jiang, P. Tsai, J. Jang, J. Huang, Significantly enhanced mechanical properties of ZrAlCo bulk amorphous alloy by microalloying with Ta, Intermetallics 93 (2018) 162–168.
[17] J.J. Lewandowski, W.H. Wang, A.L. Greer, Intrinsic plasticity or brittleness of metallic glasses, Philos. Mag. Lett. 85 (2) (2005) 77–87.
[18] X.J. Gu, A.G. Mcdermott, S. Joseph Poon, G.J. Shiflet, Critical Poisson's ratio for plasticity in Fe-Mo-C-B-Ln bulk amorphous steel, Appl. Phys. Lett. 88 (23) (2006) 211905.
[19] Y.H. Liu, G. Wang, R.J. Wang, D.Q. Zhao, M.X. Pan, W.H. Wang, Super plastic bulk metallic glasses at room temperature, Science 315 (5817) (2007) 1385–1388.
[20] L.Y. Chen, A.D. Setyawan, H. Kato, A. Inoue, G.Q. Zhang, J. Saida, X.D. Wang, Q.P. Cao, J.Z. Jiang, Free-volume-induced enhancement of plasticity in a monolithic bulk metallic glass at room temperature, Scr. Mater. 59 (1) (2008) 75–78.
[21] S.H. Xie, X.R. Zeng, H.X. Qian, Correlations between the relaxed excess free volume and the plasticity in Zr-based bulk metallic glasses, J. Alloy. Compd. 480 (2) (2009) L37–L40.
[22] J.W. Liu, Q.P. Cao, L.Y. Chen, X.D. Wang, J.Z. Jiang, Shear band evolution and hardness change in cold-rolled bulk metallic glasses, Acta Mater. 58 (14) (2010) 4827–4840.
[23] Y. Tan, Y.W. Wang, X.W. Cheng, Q. Fu, Z.H. Xin, Z.Q. Xu, H.W. Cheng, Effects of Al replacement on glass forming ability and mechanical properties of Zr-based bulk metallic glasses, J. Non-Cryst. Solids 568 (2021) 120962.
[24] O. Haruyama, K. Kisara, A. Yamashita, K. Kogure, Y. Yokoyama, K. Sugiyama, Characterization of free volume in cold-rolled Zr55Cu30Ni5Al10 bulk metallic glasses, Acta Mater. 61 (9) (2013) 3224–3232.
[25] M. Stolpe, J.J. Kruzic, R. Busch, Evolution of shear bands, free volume and hardness during cold rolling of a Zr-based bulk metallic glass, Acta Mater. 64 (64) (2014) 231–240.
[26] L.Y. Chen, Z.D. Fu, G.Q. Zhang, X.P. Hao, Q.K. Jiang, X.D. Wang, Q.P. Cao, H. Franz, Y.G. Liu, H.S. Xie, New class of plastic bulk metallic glass, Phys. Rev. Lett. 100 (7) (2008) 075501.
[27] W. Zhou, J. Hu, W. Weng, L. Gao, G. Xu, Enhancement of plasticity in Zr-Cu-Ni-Al-Ti bulk metallic glass by heterogeneous microstructure, J. Non-Cryst. Solids (2018) 530–536.
[28] N. Zheng, R.T. Qu, S. Pauly, M. Calin, T. Gemming, Z.F. Zhang, J. Eckert, Design of ductile bulk metallic glasses by adding "soft" atoms, Appl. Phys. Lett. 100 (14) (2012) 1085.
[29] Z. Lu, C. Liu, Role of minor alloying additions in formation of bulk metallic glasses: a review, J. Mater. Sci. 39 (12) (2004) 3965–3974.
[30] W.H. Wang, Roles of minor additions in formation and properties of bulk metallic glasses, Prog. Mater. Sci. 52 (4) (2007) 540–596.
[31] L. Deng, B. Zhou, H. Yang, X. Jiang, B. Jiang, X. Zhang, Roles of minor rare-earth elements addition in formation and properties of Cu-Zr-Al bulk metallic glasses, J. Alloy. Compd. 632 (2015) 429–434.
[32] Y. Liu, G. Wang, H. Li, S. Pang, K. Chen, T. Zhang, TiCuZrFeSnSiSc bulk metallic glasses with good mechanical properties for biomedical applications, J. Alloy. Compd. 679 (2016) 341–349.
[33] J. Zhu, C. Wang, J. Han, S. Yang, G. Xie, H. Jiang, Y. Chen, X. Liu, Formation of Zr-based bulk metallic glass with large amount of yttrium addition, Intermetallics 92 (2018) 55–61.
[34] A.A. Kundig, A.J. Perry, P.J. Uggowitzer, Influence of low oxygen contents and alloy refinement on the glass forming ability of Zr52.5Cu17.9Ni14.6Al10Ti5, Mater. Trans. 43 (12) (2002) 3206–3210.
[35] F. Jiang, Z.J. Wang, Z.B. Zhang, J. Sun, Formation of Zr-based bulk metallic glasses from low purity materials by scandium addition, Scr. Mater. 53 (5) (2005) 487–491.
[36] S.H. Wang, H.K. Pei, H.T. Tsang, R.J. Rong, L.L. Yu, The influence of Sc addition on the welding microstructure of Zr-based bulk metallic glass: the stability of the amorphous phase, Appl. Phys. Lett. 91 (17) (2007) 26–36.
[37] H. Cao, D. Ma, K.C. Hsieh, L. Ding, W.G. Stratton, P.M. Voyles, Y. Pan, M. Cai, J.T. Dickinson, Y.A. Chang, Computational thermodynamics to identify Zr-Ti-Ni-Cu-Al alloys with high glass-forming ability, Acta Mater. 54 (2006) 2975–2982.
[38] R.D. Conner, Y. Li, W.D. Nix, W.L. Johnson, Shear band spacing under bending of Zr-based metallic glass plates, Acta Mater. 52 (8) (2004) 2429–2434.
[39] Y. Wu, D. Cao, Y.L. Yao, G.S. Zhang, J.Y. Wang, L.Q. Liu, F.S. Li, H.Y. Fan, X.J. Liu, H. Wang, X.Z. Wang, H.H. Zhu, S.H. Jiang, P. Kontis, D. Raabe, B. Gault, Z.P. Lu, Substantially enhanced plasticity of bulk metallic glasses by densifying local atomic packing, Nat. Commun. 12 (2021) 6582.
[40] M.C. Li, H.M. Guan, S. Yang, X. Ma, Q. Li, Minor Cr alloyed Fe-Co-Ni-P-B high entropy bulk metallic glass with excellent mechanical properties, Mater. Sci. Eng. A 805 (2021) 140542.
[41] E.J. Huber, G.C. Fitzgibbon, E.L. Head, C.E. Holley, J. Phys. Chem. 67 (1963) 1731.
[42] F.R. De Boer, W. Mattens, R. Boom, A. Miedema, A. Niessen, Cohesion in Metals, (1988).
[43] D. Wang, Y. Li, B.B. Sun, M.L. Sui, K. Lu, E. Ma, Appl. Phys. Lett. 84 (2004) 4029–4031.
[44] Y.C. Hu, H. Tanaka, Physical origin of glass formation from multicomponent systems, Sci. Adv. 6 (2020) eabd2928.
[45] F. Guo, S.J. Poon, G.J. Shiflet, Metallic glass ingots based on yttrium, Appl. Phys. Lett. 83 (2003) 2575.
[46] B. Zhang, R.J. Wang, D.Q. Zhao, M.X. Pan, W.H. Wang, Properties of Ce -based bulk metallic glass-forming alloys, Phys. Rev. B 70 (22) (2004) 35–40.
[47] W.H. Wang, Correlations between elastic moduli and properties in bulk metallic glasses, J. Appl. Phys. 99 (9) (2006) 1947-135.
[48] S.W. Lee, M.Y. Huh, E. Fleury, J.C. Lee, Crystallization-induced plasticity of Cu-Zr containing bulk amorphous alloys, Acta Mater. 54 (2) (2006) 349–355.
[49] L.Z. Zhao, R.J. Xue, Z.G. Zhu, Z. Lu, E. Axinte, W.H. Wang, H.Y. Bai, Evaluation of flow units and free volumes in metallic glasses, J. Appl. Phys. 116 (2014) 103516.
[50] A. Gulzar, L.Z. Zhao, R.J. Xue, K. Shahzad, D.Q. Zhao, W.H. Wang, Correlation between flow units and crystallization in metallic glasses, J. Non-Cryst. Solids 461 (2017) 61–66.
[51] A.V.D. Beukel, J. Sietsma, The glass transition as a free volume related kinetic phenomenon, Acta Metall. Mater. 38 (3) (1990) 383–389.
[52] A. Slipenyuk, J. Eckert, Correlation between enthalpy change and free volume reduction during structural relaxation of Zr55Cu30Al10Ni5 metallic glass, Scr. Mater. 50 (1) (2004) 39–44.
[53] P. Tuinstra, P.A. Duine, J. Sietsma, The glass transition for as-quenched and pre-annealed amorphous Pd40Ni40P20, measured and explained, J. Non-Cryst. Solids 156 (1993) 519–522.
[54] J. Pan, Yu.P. Ivanov, W.H. Zhou, Y. Li, A.L. Greer, Strain-hardening and suppression of shear-banding in rejuvenated bulk metallic glass, Nature 578 (2020) 559–562.
[55] S.V. Ketov, Y.H. Sun, S. Nachum, Z. Lu, A. Checchi, A.R. Beraldin, H.Y. Bai, W.H. Wang, D.V. Louzguine-Luzgin, M.A. Carpenter, A.L. Greer, Rejuvenation of metallic glasses by non-affine thermal strain, Nature 524 (2015) 200–203.
[56] H. Kato, H.S. Chen, A. Inoue, Relationship between thermal expansion coefficient and glass transition temperature in metallic glasses, Scr. Mater. 58 (12) (2008) 1106–1109.
[57] J.C. Ye, J. Lu, C.T. Liu, Q. Wang, Y. Yang, Atomistic free-volume zones and inelastic deformation of metallic glasses, Nat. Mater. 9 (8) (2010) 619–623.
[58] F. Spaepen, Homogeneous flow of metallic glasses: a free volume perspective, Scr. Mater. 54 (2006) 363–367.
[59] F. Spaepen, A microscopic mechanism for steady state inhomogeneous flow in metallic glasses, Acta Met. 25 (4) (1976) 407–415.